

Elsevier required licence: © 2021

This manuscript version is made available under the
CC-BY-NC-ND 4.0 license

<http://creativecommons.org/licenses/by-nc-nd/4.0/>

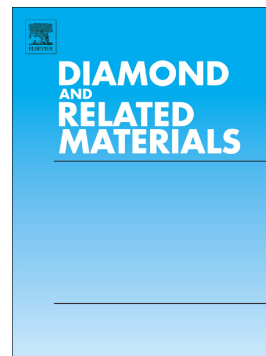
The definitive publisher version is available online at

<https://doi.org/10.1016/j.diamond.2020.108210>

Journal Pre-proof

Evaluation of Electrocatalytic Dinitrogen Reduction Performance on Diamond Carbon via Density Functional Theory

Zhongyuan Guo, Siyao Qiu, Huan Li, Yongjun Xu, Steven J. Langford, Chenghua Sun



PII: S0925-9635(20)30763-9

DOI: <https://doi.org/10.1016/j.diamond.2020.108210>

Reference: DIAMAT 108210

To appear in: *Diamond & Related Materials*

Received date: 6 October 2020

Revised date: 19 November 2020

Accepted date: 20 November 2020

Please cite this article as: Z. Guo, S. Qiu, H. Li, et al., Evaluation of Electrocatalytic Dinitrogen Reduction Performance on Diamond Carbon via Density Functional Theory, *Diamond & Related Materials* (2020), <https://doi.org/10.1016/j.diamond.2020.108210>

This is a PDF file of an article that has undergone enhancements after acceptance, such as the addition of a cover page and metadata, and formatting for readability, but it is not yet the definitive version of record. This version will undergo additional copyediting, typesetting and review before it is published in its final form, but we are providing this version to give early visibility of the article. Please note that, during the production process, errors may be discovered which could affect the content, and all legal disclaimers that apply to the journal pertain.

© 2020 Published by Elsevier.

Evaluation of Electrocatalytic Dinitrogen Reduction Performance on Diamond Carbon via Density Functional Theory

Zhongyuan Guo,^{a, b} Siyao Qiu,^{a,*} Huan Li,^a Yongjun Xu,^a Steven J. Langford,^b Chenghua Sun^{b,*}

^a Science & Technology Innovation Institute, Dongguan University of Technology, Dongguan 523808, China.

^b Department of Chemistry and Biotechnology, Faculty of Science, Engineering & Technology, Swinburne University of Technology, Hawthorn, Victoria 3122, Australia

Keywords: Diamond carbon, low-coordinated carbon, electrocatalysis, NRR, density function theory

**Corresponding author:*

Dr. Siyao Qiu

Email: qiusy@dgut.edu.cn

Dr. Chenghua Sun

Email: chenghuasun@swin.edu.au

Abstract

Carbon-based electrocatalysts for nitrogen fixation under ambient conditions has attracted tremendous attention but still encounter great challenges of low Faradic efficiency (FE) and a sluggish kinetics. Inspired by intrinsic defects (vacancies, edges and dislocation) on graphene showing activity towards oxygen reduction reaction (ORR) and nitrogen reduction reaction (NRR), here, two commonly exposed surfaces of diamond carbon, i.e., C(111) & C(110), were calculated for electrocatalytic nitrogen reduction reaction (eNRR) by the density functional theory (DFT) method, and calculations show that, compared with C(110), C(111) could be highly promising towards eNRR with a low over-potential (η) of 0.57 V ($\Delta G_{\max} = 0.73$ eV, $\eta = 0.57$ V), which are distinctly less than that ($\Delta G_{\max} = 1.06$ eV, $\eta = 0.92$ V) of flat benchmark Ru(0001) catalysts. Importantly, these two surfaces are shown to exhibit the suppression of hydrogen evolution reaction (HER). This work is the first reported indication that the low-coordinated carbons (LCCs) on sp^3 -hybridized diamond-carbon framework are active for eNRR, which gives a brand-new direction of designing/synthesizing sp^3 -configured diamond-carbon-composited catalysts for eNRR.

1. Introduction

The nitrogen circulation, as one of the most important circles on Earth, exerts great impact on human beings and other organisms [1]. In air, dinitrogen gas accounts for 78.1% of air composition [2], however, the huge utilization of elemental nitrogen from air, i.e. nitrogen fixation, is not easy. Naturally, some microorganisms can convert N_2 to ammonia using nitrogenases [3]; some N-containing compounds can also be formed in electrical storms [1, 4], which can be used by plants. But these two routes for nitrogen fixation are not enough for meeting the demands of social development. Currently, artificial nitrogen fixation heavily relies

on the Haber-Bosch (H-B) process, which occurs under high temperature and pressure with the massive consumption of global energy and significant emission of greenhouse gases [5]. Facing the world growing energy crisis and changes in global climate, searching for a sustainable substitution for the transitional H-B process is highly desirable.

Electrochemical nitrogen fixation has been regarded as the most promising route for the synthesis of ammonia in that it can convert N_2 and water into ammonia on active sites of electrocatalysts using renewable electricity, such as from wind and solar sources, without the added release of CO_2 in coal-fired power stations [6, 7]. However, the performance of electrocatalysts to date is still far from pragmatic industrial applications due to the large challenges of low FE and production rate of ammonia areas which have already attracted tremendous attention from scientists [8-16].

Defect engineering has been adopted in recent years as a universal strategy to tailor catalyst materials for specific and demanding reactions [17-22]. Moreover, reviewing defect electrocatalytic mechanisms further deepens the understanding of the defect mechanism concept - starting from the common concept of heteroatom doping to a new concept of topological defects and then facilitates the subsequent rational design of advanced electrocatalysts [20]. Of special interest are the intrinsic defects on the edge of graphene or basal plane holes that are active for oxygen reduction, evidenced by the subtle measurement device of a micro-electrochemical testing system, which, for the first time, suggests that LCCs are active due to the different charge distribution of the basal-plane hole or edge with that of the basal plane [23]. More recently, intrinsic defects (vacancies and dislocation) within LCCs on graphene were investigated to show promising activity towards eNRR [24]. Inspired by those works, designing electrocatalysts

intentionally with such defects/active sites in the low-coordination environment should be highly effective.

Carbon-based electrocatalysts have been intensively investigated for electrochemical nitrogen reduction due to their catalytic potentials, stabilities and abundant storages on Earth compared with metal-based ones [25-31]. For example, the pioneering work of B-doped graphene for electrocatalytic nitrogen reduction reaction (eNRR) by Yu *et al.* [30] demonstrated an efficient metal-free carbon-based electrocatalyst for NRR; Liu *et al.* [31] reported a N-doped porous carbon with the pyrrolic and pyridinic N as active sites for the cleavage of $\text{N}\equiv\text{N}$; Moreover, graphyne-based electrocatalysts have increasingly drawn attention for designing effective eNRR catalysts due to unique physical properties and large surface area [28, 32-35]. To now, large efforts have been already devoted into designing various efficient, robust and cost-effective carbon-based electrocatalysts for NRR, but are mainly limited to sp -/ sp^2 -hybridized carbon-based materials - the sp^3 -hybridized carbon materials are rarely reported. Recently, Wanninayake *et al.* [36] demonstrated the effect of the carbon hybridization structure (sp^2/sp^3 carbon) on the electrochemical CO_2 reduction, experimentally and theoretically, which suggested the vital role of the host carbon-structure. Meanwhile, two commonly exposed surfaces of C(111) and C(110) of diamond carbon with the sp^3 -hybridized configuration for the first time were tested for eNRR by DFT, which are highly expected to show the reactivity due to LCC sites caused by dangling bonds on surface, based on the before-mentioned discussion. The theoretical results evidence that the LCC surface of sp^3 -configured diamond carbon can act as an effective metal-free electrocatalyst for eNRR with the maximum free-energy change of 0.73 eV along the associative distal pathway on C(111). We show that diamond carbon electrocatalysts display their advantages of suppressing the competing side reaction of HER, which was also observed in

boron-doped diamond carbon (BDD) electrodes for the electrocatalytic CO₂ reduction [37-39]. In addition, diamond carbon is favourably endowed with outstanding physical and chemical properties, such as high electron and hole mobilities [40], chemical stability and wide electrochemical potential window [41], making it a suitable material for pragmatic electrocatalysis applications. This research demonstrates the effect of LCCs, which can be from intrinsic and extrinsic defects on carbon-based materials, on dinitrogen reduction, and boost a brand-new direction of designing diamond carbon-composited NRR electrocatalysts.

2. Computational Details

Spin-polarized calculations were performed on (111) and (110) surfaces of ($\sqrt{3} \times \sqrt{3}$) and ($2\sqrt{2} \times \sqrt{3}$) supercells (catalysts models are shown in Fig. 1) of diamond carbon, with lattice parameters of $a = b = 8.75 \text{ \AA}$, $\alpha = \beta = 90^\circ$, $\gamma = 60^\circ$, and $a = b = 8.75 \text{ \AA}$, $\alpha = \beta = 90^\circ$, $\gamma = 70.5^\circ$, respectively, using DMol³ code available in the Materials Studio package [42, 43]. The thickness of vacuum is set to 20 \AA to avoid possible interaction in the z -direction. The two surface models investigated all have five layers, with the bottom two fixed during geometry optimization. Revised Perdew-Burke-Ernzerhof exchange-correlation functional [44] of the generalized gradient approximation was used to describe the interaction amongst electrons. Effective core potentials [45, 46] was chosen as the pseudopotential, and double numerical basis sets with polarization functions (DNP) was adopted as the atomic orbital basis set. A k-point set of $3 \times 3 \times 1$ was used to sample the Brillouin zone for geometry optimization, and the real-space global cutoff radius set to 5.2 \AA . Each geometry optimization was performed until the maximum force was below 0.002 Ha/ \AA , energy tolerance below 10^{-5} Ha, and maximum displacement below 0.005 \AA . The Gibbs free-energy change (ΔG) of each elementary step at 298.15 K for eNRR was

performed based on the standard hydrogen electrode (SHE) [47-49], where the free-energy of H^+/e^- pair equals half of that of a hydrogen molecule, as follows:

$$\Delta G = \Delta E_{\text{DFT}} + \Delta E_{\text{ZPE}} - T \cdot \Delta S + \Delta G_U + \Delta G_{\text{pH}}$$

where ΔE_{DFT} is the DFT electron energy difference after structural convergence, ΔE_{ZPE} and ΔS are changes of the zero-point energy and entropy, respectively. Here, Free-energy correction is based on the ZPE of reaction intermediates, obtained from the frequency analyses (see Table S2 and S3). As for the entropies of intermediates, their contributions are negligible compared to the free gas molecules and thus TS of reaction intermediates is equal to zero. ΔG_U is the contribution from applied electrode potential U . ΔG_{pH} is the free-energy correction of H^+ by the concentration with the equation of $\Delta G_{\text{pH}} = 2.303 \times k_B T \times \text{pH}$, where k_B is the Boltzmann constant and the pH is set as zero (strong acidic environment). The limiting potential (U_L) of the whole process of eNRR is obtained according to $U_L = -\text{Max}(\Delta G_i)/e$, and the corresponding over-potential (η) is defined as: $\eta = U_e (-0.16 \text{ V}) - U_L$, with U_e representing the equilibrium potential of NRR ($N_2 + 6H^+ + 6e^- \rightarrow 2NH_3$) vs. Standard Hydrogen Electrode (SHE). For obtaining details regarding to the interaction between dinitrogen and the catalyst, electron density difference and projected density of states (PDOS). Hirshfeld and Mulliken charge analyses of the intermediate *NN were performed in the CASTEP code.

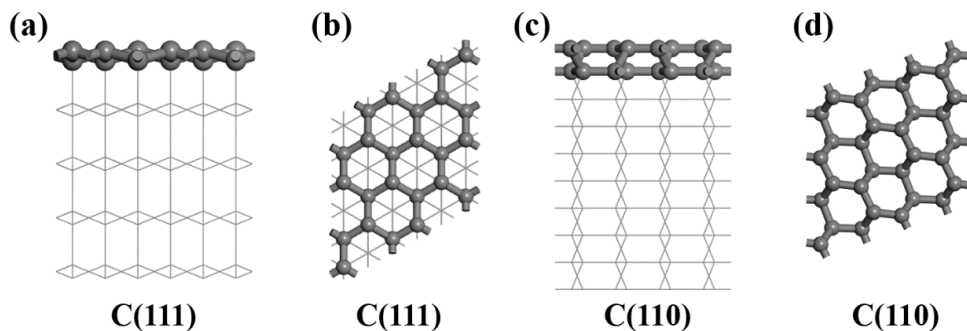


Fig. 1. Surface models of diamond carbon: (a) and (c) are the side views; (b) and (d) are the top views.

3. Results and Discussion

3.1. Nitrogen chemisorption on C(111) and C(110)

Nitrogen capture and activation plays a critical role in the eNRR process [50], which can directly affect subsequent hydrogenation of the $\text{N}\equiv\text{N}$ bond and thus determine the activity of catalysts. Fig. 2 displays three adsorption configurations of dinitrogen on C(111) and C(110) and corresponding N-N bond length after adsorption. For more clarity on N_2 adsorption configurations, the bare surfaces and corresponding structures are displayed in Fig. S1. According to the adsorption energy (E_{ads}) equation: $E_{\text{ads}} = E_{\text{N}_2/\text{slab}} - E_{\text{slab}} - E_{\text{N}_2}$, where $E_{\text{N}_2/\text{slab}}$, E_{slab} and E_{N_2} represent the total electron energy of the whole composite system after adsorption, the slab model and a free N_2 molecule, respectively, E_{ads} of dinitrogen on C(111) and C(110) were calculated. In Fig. 2, it can be seen that $\text{N}\equiv\text{N}$ bond was elongated in the tilt end-on way from the initial 1.11 Å of a free N_2 molecule to average 1.25 Å of *NN, suggesting the $\text{N}\equiv\text{N}$ bond is well-activated. The adsorption energy calculations suggest that the N_2 adsorption on C(111), as shown in Fig. 2(a) can be readily realized with $E_{\text{ads}} = -0.14$ eV, while E_{ads} on C(110) are positive, i.e. 1.72 and 0.47 eV, respectively, for Fig. 2(b) and 2(c), respectively, indicating the extra energy input is needed to stabilize N_2 adsorption. Note that due to the high density of active sites on C(111) and C(110), the N_2 molecule prefers to be captured in the tilt end-on way energetically after geometry optimizations.

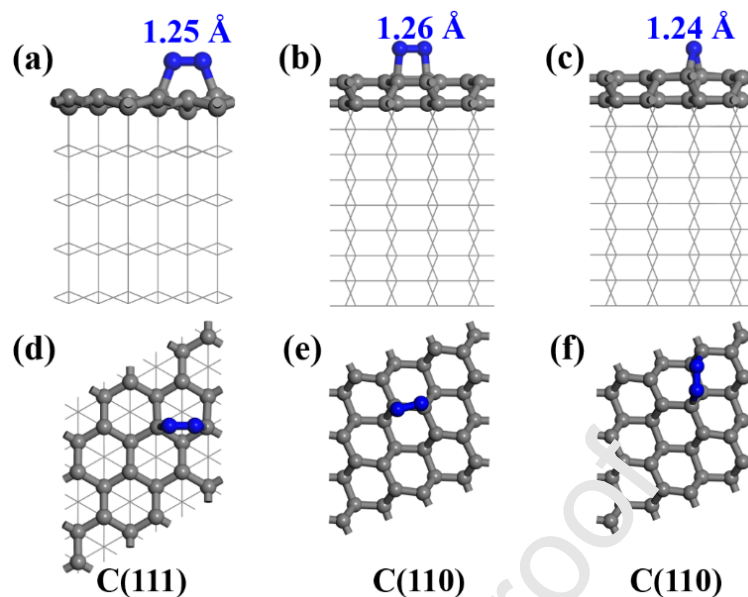


Fig. 2. Adsorption models of dinitrogen on C(111) and C(110). Fig. (a)-(c) display the side views and Fig. (d)-(f) display the top views. N-N bond lengths are shown in blue in the unit of Å.

C and N are shown as grey and blue spheres, respectively.

Fig. 3 displays the corresponding changes of electron density after N_2 adsorption on C(111) and C(110). In its entirety, there exists strong electron interactions/transfer between N_2 and catalysts. More specifically, the electron density between two nitrogen atoms decreases upon the adsorption of N_2 , suggesting the $N\equiv N$ bond is weakened, which is also supported by the elongation of the $N\equiv N$ bond shown in Fig. 2. Meanwhile, Mulliken and Hirshfeld charge analyses [51] (see Table S1) both quantitatively show adsorbed $*NN$ species possess the negative charges, which would be transferred to the anti-bonding orbital $1\pi^*$ of N_2 and thus activate the stable $N\equiv N$ bond due to the electron back-donation effect [52, 53].

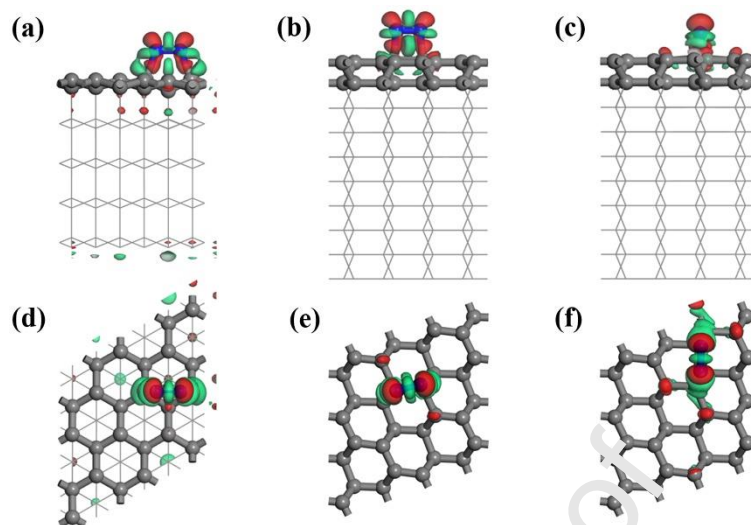


Fig. 3. Diagram of electron density difference of adsorbed N_2 on C(111) and C(110). The red and green regions represent the electron accumulation and loss, respectively (Isosurface = 0.05 a.u.).

In order to investigate the origin of existing interactions between dinitrogen and these two catalytic C(111) and C(110) surfaces, the PDOS of active carbon atoms bonded directly to N atoms (detailed indication in Fig. S2) and adsorbed dinitrogen were calculated and displayed in Fig. 4. The overlap area between the PDOS of the active carbon and that of *NN from the range of -5 to 0 eV is noted, which suggests the strong interaction between dinitrogen and catalytic surfaces exists [54]. These results agree well with the electron transfer from the electron density difference of adsorbed *NN (see Fig. 3). Moreover, it is also noticeable that, compared with the highest peak position of active carbon atoms in the energy range of -2.5 to 0 eV shown in Fig. 4(c), the highest peak of active carbon atoms in the same energy range shown in Fig. 4(b) moves towards the energy-negative direction. Generally, a lower peak position indicates the antibonding states are with a higher occupancy, thus resulting in the increase of a system energy and then low affinity to adsorbates [29, 55]. Therefore, these two PDOS profiles in Fig. 4(b) and 4(c) well explain the big difference on N_2 adsorption energies on C(110), and N_2 will prefer to react

with C(110) surface through the latter model energetically (shown in Fig. 2(c) (side view) and 2(f) (top view)) compared with the former model (shown in Fig. 2(b) (side view) and 2(e) (top view)), although the reaction still needs extra acceptable energy input. In addition, the PDOS of active carbon atoms and N atoms were also projected on the s - and p -orbital of elements, as shown in Fig. S3 and S4, from which we can know the interaction between dinitrogen and the catalytic surface mainly originates from the p - p orbital-coupling, different from the d - p orbital interaction on metal-based electrocatalysts.

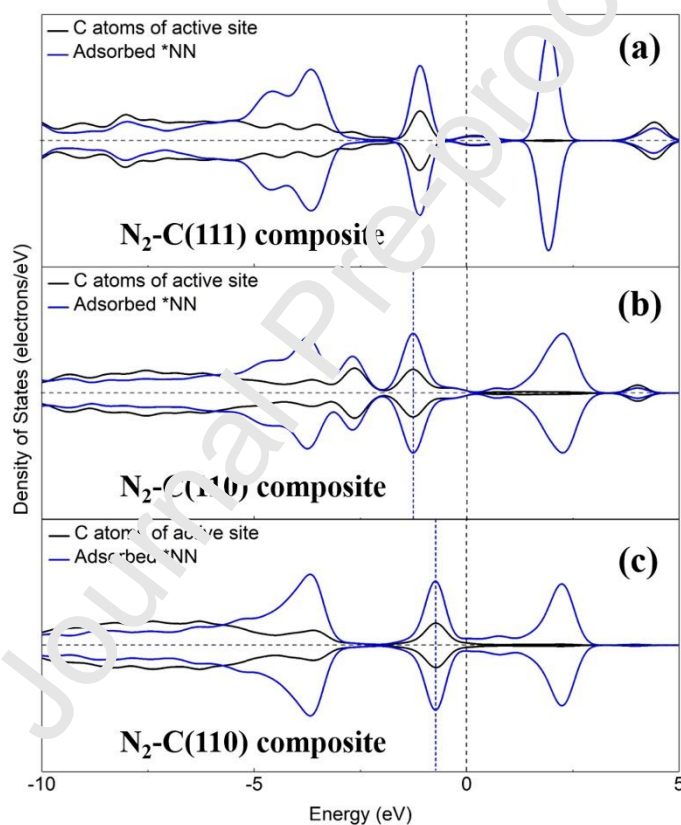


Fig. 4. PDOS of the C atoms directly bonded to N_2 and adsorbed *NN on C(111) (a) and C(110) (b, c), as displayed in Fig. 2 (a), 2(b) and 2(c), respectively. The presentation of active C atoms that directly bonded to N_2 is shown in Fig. S2, in detail.

3.2. NRR on diamond carbon

According to previous reports, there exist three different reaction pathways for eNRR, i.e., distal, alternating and enzymatic mechanisms [56]. Enzymatic mechanism usually occurs when dinitrogen adsorbs on the active site through the side-on model, then six pairs of H^+/e^- alternatively attack the N atoms, finally forming two NH_3 molecules released from the active site.

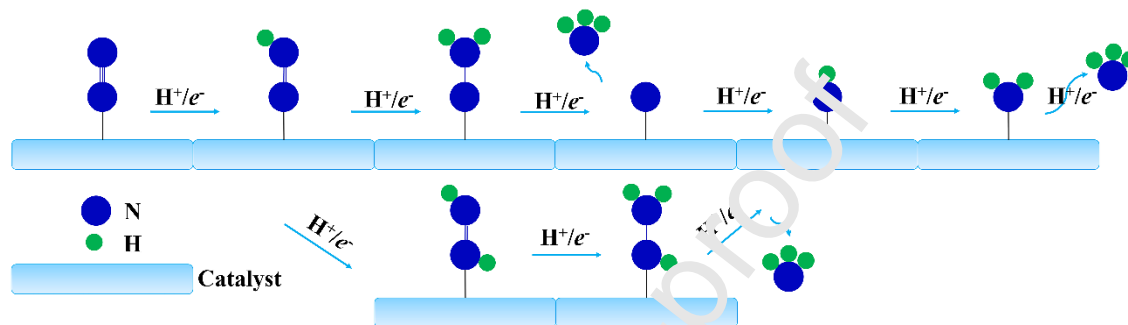


Fig. 5. Schematic illustration of distal and alternating pathways for nitrogen reduction reaction on electrocatalysts.

In our interpretation, only the distal and alternating reaction pathways, as shown in Fig. 5, are taken into account considering the tilt end-on adsorption models of dinitrogen on C(111) and C(110). For the distal pathway, the H^+/e^- first attacks the distal N atom of adsorbed $*NN$ till the formation of first NH_3 , then leaving $*N$ species for the subsequent reduction into the second NH_3 , and finally the recovered active site will be involved in the next dinitrogen reduction cycle; while for alternating one, the difference with the distal pathway is the alternating hydrogenation starting from the step $*NNH + H^+ + e^- \rightarrow *NHNH$.

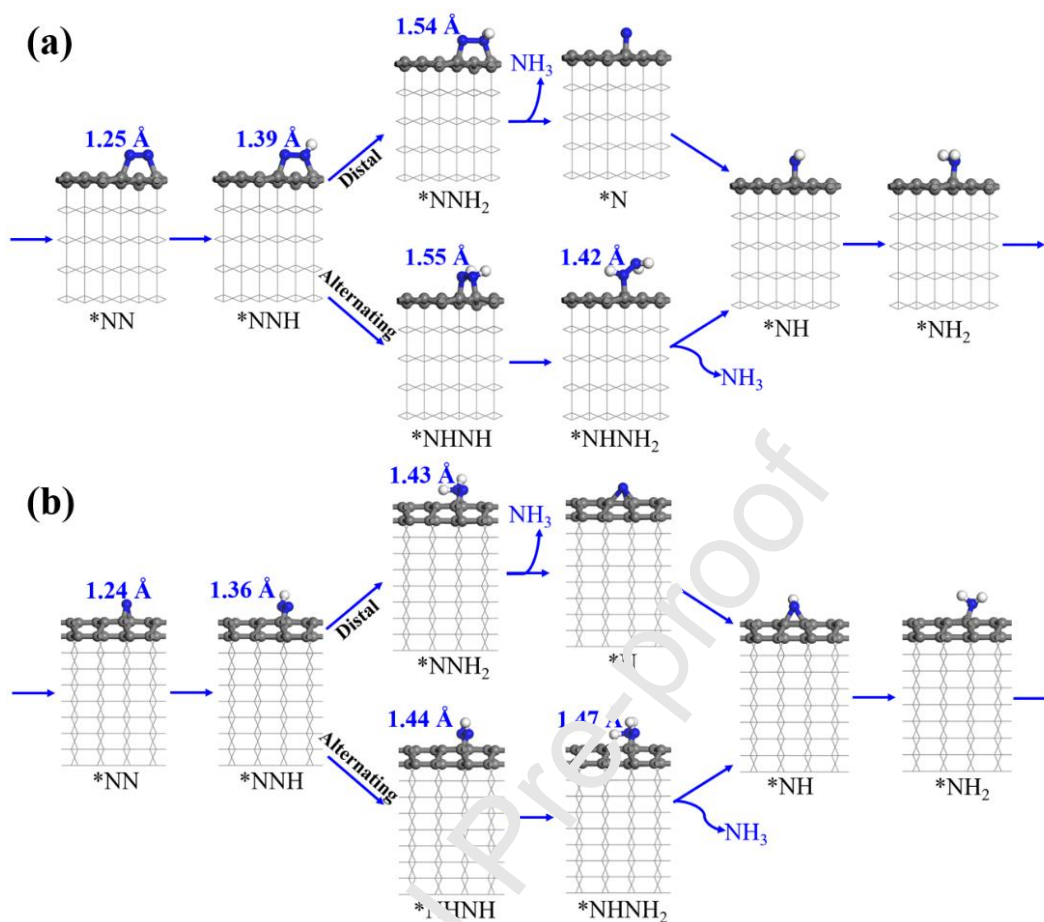


Fig. 6. Electrocatalytic NRR pathways on (a) C(111) and (b) C(110). The evolution of N-N bond length is shown through blue labels in the unit of Å.

In Fig. 6(a), the reaction intermediates on C(111) along the reaction pathway is shown starting from the N₂ adsorption. However, on C(110), dinitrogen could have two adsorption models on C(110) based on before-mentioned discussion on N₂ capture and activation, but the latter adsorption configuration model, as shown in Fig. 2(c), is more likely to occur due to the more energetically favourable adsorption energy in comparison with that of the former one (Fig. 2(b)). Therefore, the latter is regarded as the starting point for eNRR. In Fig. 6(b) could be seen the whole eNRR pathways, including distal and alternating ones, on C(110). Their corresponding free-energy evolution diagrams are shown in Fig. 7. Usually, the $*\text{NN} + \text{H}^+ + e^- \rightarrow *\text{NNH}$ (first

hydrogenation) step is of significantly crucial on the grounds that the first hydrogenation is often a potential-determining step according to previous reports [10, 57, 58]. However, in Fig. 7, we can see the free-energy change of the first hydrogenation step on C(111) is very small, just 0.17 eV, and even negative on C(110), showing the $\text{N}\equiv\text{N}$ bond is well-activated on these two catalytic surfaces, as evidenced by the largely elongated N-N bond length of absorbed $^*\text{NN}$ in Fig. 2. With the successive attack of H^+/e^- pairs, the N-N length evolution of $^*\text{N}_x\text{H}_y$ species is shown in Fig. 6 till the release of the first NH_3 formed on C(111) and C(110). In Fig. 6, it is seen that the N-N length is gradually increased except the diazene step of $^*\text{NHNH} + \text{H}^+ + \text{e}^- \rightarrow ^*\text{NHNH}_2$ on C(111), representing the increasingly weakened interaction between two N adatoms during eNRR. This increasingly weakened interaction on the N-N bond is very beneficial to eNRR by proton-coupled electron transfer (PCET), because it can avoid resulting in the step with an extremely large limiting potential. In Fig. 7, we can see the free-energy evolution of eNRR on C(111) and C(110) along the reaction coordination. The step with the maximum free-energy change is regarded as a potential-determining step during eNRR. To be specific, the maximum free-energy change through distal pathway is 0.73 eV from the step of $^*\text{NNH}_2 + \text{H}^+ + \text{e}^- \rightarrow ^*\text{N} + \text{NH}_3$ on C(111), while the maximum free-energy change through alternating pathway is 0.78 eV of $^*\text{NHNH} + \text{H}^+ + \text{e}^- \rightarrow ^*\text{NHNH}_2$ step, which suggests eNRR would prefer the associative distal pathway on C(111). On C(110), on the other hand, the maximum free-energy change along distal/alternating pathway is from the capture and activation of N_2 with the value of 1.09 eV. Compared with C(111), the maximum free-energy change on C(110) is 49.3% higher than 0.73 eV (distal pathway), indicating that C(111) will be the better catalytic surface for eNRR under ambient conditions with $\eta = (-0.16 \text{ V}) - (-0.73 \text{ V}) = 0.57 \text{ V}$. Nonetheless, the free-energy change of eNRR on C(110) is also acceptable compared with some early transition metal surfaces

($\Delta G_{\max} = 1.00 \sim 1.50$ eV) [58] and experimentally reported NRR electrocatalysts [34, 59], and also very close to the case of flat Ru(0001) benchmark catalysts ($\Delta G_{\max} = 1.08$ eV) [60]. To obtain more convincing comparisons, the calculation should try to be based on the same method. The recent predicted single-atom N-doped graphene-supported catalysts [61] like Ti@N₄ ($U_L = -0.69$ V, $\eta = 0.53$ V) and V@N₄ ($U_L = -0.87$ V, $\eta = 0.71$ V) with the same RPBE exchange-correlation functional show comparable results with that on C(111) of diamond carbon ($U_L = -0.73$ V, $\eta = 0.57$ V), therefore suggesting the LCCs surface of diamond carbon could be promising for eNRR.

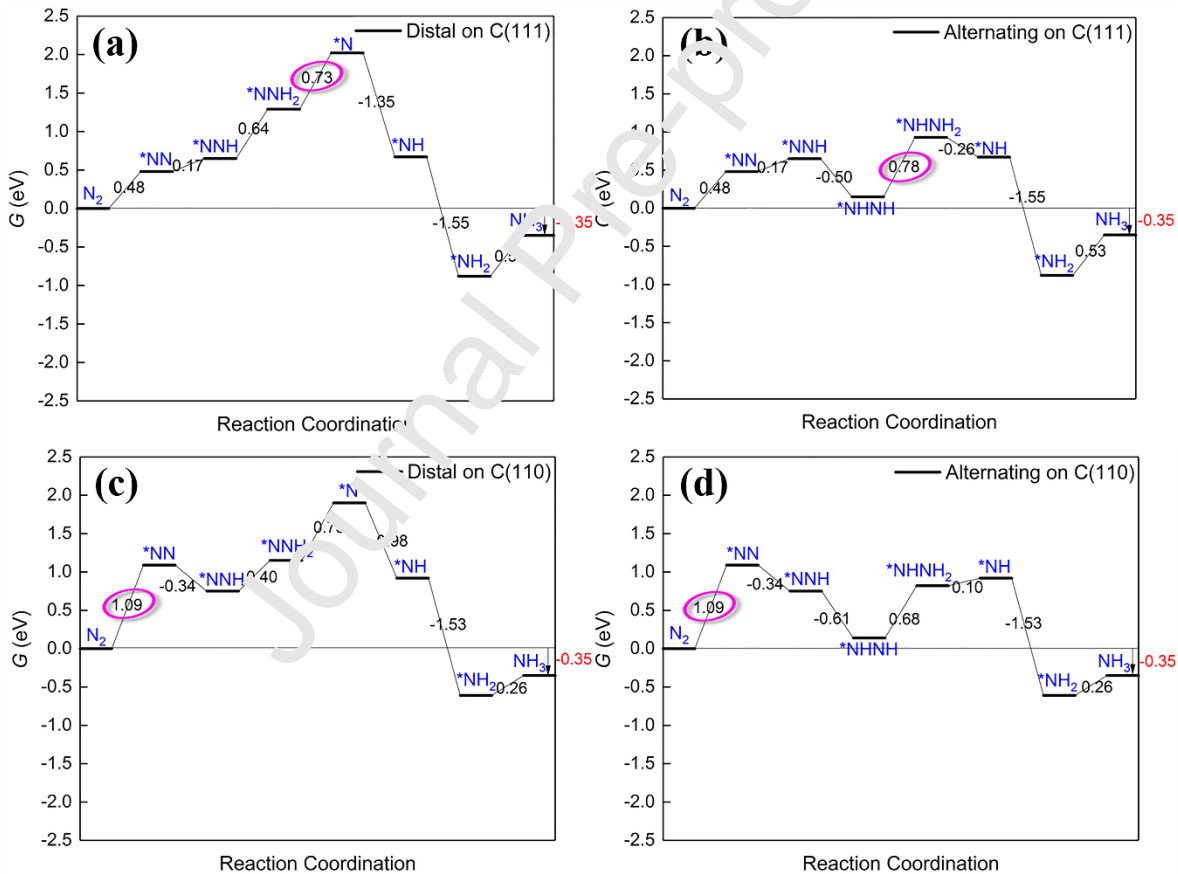


Fig. 7. (a) and (b) Energy profiles of distal and alternating pathway on C(111), respectively; (c) and (d) Energy profiles of distal and alternating pathway on C(110), respectively. The energy

values are marked in red circles for potentially rate-determining elementary steps of distal and alternating reaction pathways on C(111) and C(110).

3.3. Hydrogen evolution reaction

In the environment of an electrochemical solution, the proton from water can be adsorbed on the electrode under the same region of negative voltage to form hydrogen gas during the eNRR process, consequently lowering the yield of ammonia and FE [9, 62]. Therefore, it is an important consideration to test the dominant side reaction (HER) during the process of electrocatalytic dinitrogen reduction. In Fig. 8, calculated HER free-energy profiles on C(111) and C(110) in acidic environment are shown with the free-energy changes of -1.86 and -1.28 eV, respectively. Obviously, the release of hydrogen adsorbed on surface is relatively difficult and then HER performance can be well-suppressed due to the larger free-energy than those of eNRR on C(111) and C(110). Therefore, a sluggish HER kinetics expected would lead to a satisfactory eNRR performance with a higher selectivity into NH_3 synthesis on both two surfaces of diamond carbon when a negative bias is applied.

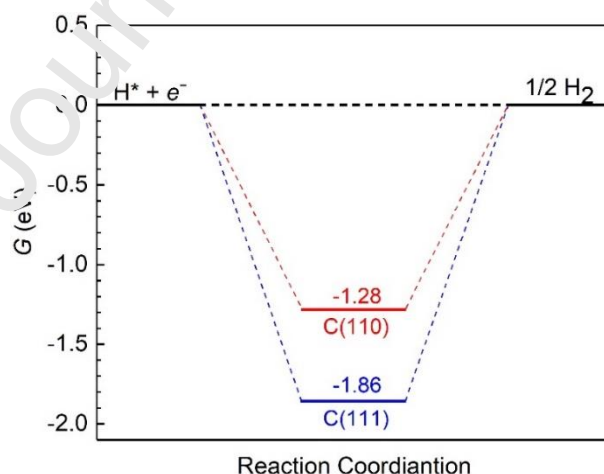


Fig. 8. Energy profiles of HER on C(111) and C(110).

Additionally, according to the previous report [63], H-terminated surface of diamond carbon has the negative electron affinity (NEA), which means it can become a solid-state emitter of electrons when illuminated with ultraviolet lights. Moreover, Hamers *et al.* [64, 65] showed that the solvated electrons in water can initiate energy-intensive reactions as energetic reducing agents. Therefore, based on working mechanism of metal-assisted NEA photoemission [66] in which excited metals inject electrons into the conduction band of diamond, it is expected that solvated electron in water can be more efficiently induced under the negative bias through electron transfer from the metal substrate to the diamond film when illuminated with ultraviolet lights. As depositing catalysts onto conductive substrates is a common strategy to enhance electrochemical reactions and the maximum free-energy change of the alternating pathway on C(111) is lower than that on C(110), C(111) surface would be highly promising to dinitrogen reduction as a photoelectrocatalyst when some hydrogen atoms cover the catalytic surface in electrolyte.

4. Conclusion

In summary, two commonly exposed C(111) and C(110) surfaces of sp^3 -hybridized diamond carbon were investigated for eNRR by DFT method, and calculation results indicate that the sp^3 -configured low-coordinated carbon is active for dinitrogen capture and reduction with moderate free-energy changes. Especially, together with the sluggish HER due to larger free-energy changes for the release of absorbed hydrogen, the C(111) surface of diamond carbon is expected to be highly promising for eNRR under electrolysis. In detail, compared with C(110), the eNRR energetically prefers to occur on C(111) through the associative distal pathway with a low over-potential of just 0.57 V, which is obviously less than that of flat Ru(0001) benchmark ($U_L = -1.08$ V, $\eta = 0.92$ V) and close to recently reported metal single-atom catalysts. Lastly, this

work would boost a new direction for designing diamond-carbon-composited NRR electrocatalysts.

Conflicts of interest

The authors declare that they have no known competing financial interests or personal relationships that could have appeared to influence the work reported in this paper.

Acknowledgements

The authors acknowledge the financial support by Guangdong Innovation Research Team for Higher Education (2017KCXTD030) and High-level Talents Project of Dongguan University of Technology (KCYKYQD2017017) and Engineering Research Center of None-food Biomass Efficient Pyrolysis and Utilization Technology of Guangdong Higher Education Institutes (2016GCZX009) and Research Center of New Energy Materials (KCYCXPT2017005). The authors also thank the National Computational Infrastructure (NCI), which is supported by the Australian Government, for providing the computational resources.

References

- [1] D. Fowler, M. Coyle, U. Skiba, M.A. Sutton, J.N. Cape, S. Reis, L.J. Sheppard, A. Jenkins, B. Grizzetti, J.N. Galloway, P. Vitousek, A. Leach, A.F. Bouwman, K. Butterbach-Bahl, F. Dentener, D. Stevenson, M. Amann, M. Voss, The global nitrogen cycle in the twenty-first century. *Philos. Trans. R. Soc. B* 368 (2013) 20130164.
- [2] T.J. Schuyler, M.I. Guzman, Unmanned aerial systems for monitoring trace tropospheric gases. *Atmosphere* 8 (2017) 206.
- [3] S.L. Foster, S.I.P. Bakovic, R.D. Duda, S. Maheshwari, R.D. Milton, S.D. Minter, M.J. Janik, J.N. Renner, L.F. Greenlee, Catalysts for nitrogen reduction to ammonia. *Nat. Catal.* 1 (2018) 490-500.

- [4] D.L. Drapcho, D. Sisterson, R. Kumar, Nitrogen fixation by lightning activity in a thunderstorm. *Atmos. Environ.* 17 (1983) 729-734.
- [5] J.W. Erisman, M.A. Sutton, J. Galloway, Z. Klimont, W. Winiwarter, How a century of ammonia synthesis changed the world. *Nat. Geosci.* 1 (2008) 636-639.
- [6] D.R. MacFarlane, P.V. Cherepanov, J. Choi, B.H.R. Suryanto, R.Y. Hodgetts, J.M. Bakker, F.M. Ferrero Vallana, A.N. Simonov, A Roadmap to the Ammonia Economy. *Joule* 4 (2020) 1186-1205.
- [7] J. Deng, J.A. Iñiguez, C. Liu, Electrocatalytic Nitrogen Reduction at Low Temperature. *Joule* 2 (2018) 846-856.
- [8] Y. Huang, D.D. Babu, Z. Peng, Y. Wang, Atomic Modulation, Structural Design, and Systematic Optimization for Efficient Electrochemical Nitrogen Reduction. *Adv. Sci.* 7 (2020) 1902390.
- [9] G.F. Chen, S. Ren, L. Zhang, H. Cheng, Y. Luo, K. Zhu, L.X. Ding, H. Wang, Advances in Electrocatalytic N₂ Reduction—Strategies to Tackle the Selectivity Challenge. *Small Methods* 3 (2018) 1800337.
- [10] J. Wang, S. Chen, Z. Li, C. Li, X. Liu, Recent Advances in Electrochemical Synthesis of Ammonia through Nitrogen Reduction under Ambient Conditions. *ChemElectroChem* 7 (2020) 1067-1079.
- [11] B.H.R. Suryanto, H.-L. Du, D. Wang, J. Chen, A.N. Simonov, D.R. MacFarlane, Challenges and prospects in the catalysis of electroreduction of nitrogen to ammonia. *Nat. Catal.* 2 (2019) 290-296.

- [12] Z. Jin, C. Liu, Z. Liu, J. Han, Y. Fang, Y. Han, Y. Niu, Y. Wu, C. Sun, Y. Xu, Rational Design of Hydroxyl-Rich $\text{Ti}_3\text{C}_2\text{T}_x$ MXene Quantum Dots for High-Performance Electrochemical N_2 Reduction. *Adv. Energy Mater.* 10 (2020) 2000797.
- [13] Q. Li, C. Liu, S. Qiu, F. Zhou, L. He, X. Zhang, C. Sun, Exploration of iron borides as electrochemical catalysts for the nitrogen reduction reaction. *J. Mater. Chem. A* 7 (2019) 21507-21513.
- [14] X. Wang, S. Qiu, J. Feng, Y. Tong, F. Zhou, Q. Li, L. Song, S. Chen, K.-H. Wu, P. Su, S. Ye, F. Hou, S.X. Dou, H.K. Liu, G.Q. Lu, C. Sun, J. Liu, J. Liang, Confined Fe–Cu Clusters as Sub-Nanometer Reactors for Efficiently Regulating the Electrochemical Nitrogen Reduction Reaction. *Adv. Mater.* (2020) 2004382.
- [15] H. Niu, X. Wang, C. Shao, Z. Zhang, Y. Guo, Computational Screening Single-Atom Catalysts Supported on g-CN for N_2 Reduction: High Activity and Selectivity. *ACS Sustain. Chem. Eng.* 8 (2020) 13749-13758.
- [16] B. Liu, Y. Zheng, H.-Q. Peng, B. Ji, Y. Yang, Y. Tang, C.-S. Lee, W. Zhang, Nanostructured and Boron-Doped Diamond as an Electrocatalyst for Nitrogen Fixation. *ACS Energy Lett.* 5 (2020) 2590-2: 96.
- [17] D. Yan, Y. Li, J. Han, R. Chen, L. Dai, S. Wang, Defect Chemistry of Nonprecious-Metal Electrocatalysts for Oxygen Reactions. *Adv. Mater.* 29 (2017) 1606459.
- [18] C. Xie, D. Yan, W. Chen, Y. Zou, R. Chen, S. Zang, Y. Wang, X. Yao, S. Wang, Insight into the design of defect electrocatalysts: From electronic structure to adsorption energy. *Mater. Today* 31 (2019) 47-68.
- [19] Y. Jia, K. Jiang, H. Wang, X. Yao, The Role of Defect Sites in Nanomaterials for Electrocatalytic Energy Conversion. *Chem* 5 (2019) 1371-1397.

- [20] Y. Jia, J. Chen, X. Yao, Defect electrocatalytic mechanism: concept, topological structure and perspective. *Mater. Chem. Front.* 2 (2018) 1250-1268.
- [21] C. Xie, D. Yan, H. Li, S. Du, W. Chen, Y. Wang, Y. Zou, R. Chen, S. Wang, Defect chemistry in heterogeneous catalysis: recognition, understanding and utilization. *ACS Catal.* 10 (2020) 11082-11098.
- [22] L. Shi, Y. Yin, S. Wang, H. Sun, Rational Catalyst Design for N₂ Reduction under Ambient Conditions: Strategies toward Enhanced Conversion Efficiency. *ACS Catal.* 10 (2020) 6870-6899.
- [23] A. Shen, Y. Zou, Q. Wang, R.A.W. Dryfe, X. Huang, S. Dou, L. Dai, S. Wang, Oxygen Reduction Reaction in a Droplet on Graphite: Direct Evidence that the Edge Is More Active than the Basal Plane. *Angew. Chem. Int. Ed.* 53 (2014) 10804-10808.
- [24] F. Wang, X. Xu, J. Mao, Can graphene with intrinsic defects electrocatalyze N₂ to NH₃ reduction? *Diamond Relat. Mater.* 109 (2020) 108037.
- [25] S. Zhao, X. Lu, L. Wang, J. Gale, P. Amal, Carbon-Based Metal-Free Catalysts for Electrocatalytic Reduction of Nitrogen for Synthesis of Ammonia at Ambient Conditions. *Adv. Mater.* 31 (2019) 1805367.
- [26] Y. Liu, Q. Li, X. Guo, X. Kong, J. Ke, M. Chi, Q. Li, Z. Geng, J. Zeng, A Highly Efficient Metal-Free Electrocatalyst of F-Doped Porous Carbon toward N₂ Electroreduction. *Adv. Mater.* 32 (2020) 1907690.
- [27] W. Qiu, X.-Y. Xie, J. Qiu, W.-H. Fang, R. Liang, X. Ren, X. Ji, G. Cui, A.M. Asiri, G. Cui, B. Tang, X. Sun, High-performance artificial nitrogen fixation at ambient conditions using a metal-free electrocatalyst. *Nat. Commun.* 9 (2018) 3485.

- [28] Q. Liu, S. Wang, G. Chen, Q. Liu, X. Kong, Activating Graphyne Nanosheet via sp-Hybridized Boron Modulation for Electrochemical Nitrogen Fixation. *Inorg. Chem.* 58 (2019) 11843-11849.
- [29] K. Chu, Q.-q. Li, Y.-p. Liu, J. Wang, Y.-h. Cheng, Filling the nitrogen vacancies with sulphur dopants in graphitic C₃N₄ for efficient and robust electrocatalytic nitrogen reduction. *Appl. Catal., B* 267 (2020) 118693.
- [30] X. Yu, P. Han, Z. Wei, L. Huang, Z. Gu, S. Peng, J. Ma, G. Zheng, Boron-Doped Graphene for Electrocatalytic N₂ Reduction. *Joule* 2 (2018) 1610-1622.
- [31] Y. Liu, Y. Su, X. Quan, X. Fan, S. Chen, H. Yu, H. Zhao, Y. Zhang, J. Zhao, Facile Ammonia Synthesis from Electrocatalytic N₂ Reduction under Ambient Conditions on N-Doped Porous Carbon. *ACS Catal.* 8 (2018) 1186-1191.
- [32] T. He, S.K. Matta, A. Du, Single tungsten atom supported on N-doped graphyne as a high-performance electrocatalyst for nitrogen fixation under ambient conditions. *Phys. Chem. Chem. Phys.* 21 (2019) 1546-1551.
- [33] Y. Fang, Y. Xue, Y. Li, H. Yu, L. Hui, Y. Liu, C. Xing, C. Zhang, D. Zhang, Z. Wang, X. Chen, Y. Gao, B. Huang, Y. Li, Graphdiyne Interface Engineering: Highly Active and Selective Ammonia Synthesis. *Angew. Chem. Int. Ed.* 59 (2020) 13021-13027.
- [34] H. Zou, W. Rong, B. Long, Y. Ji, L. Duan, Corrosion-Induced Cl-Doped Ultrathin Graphdiyne toward Electrocatalytic Nitrogen Reduction at Ambient Conditions. *ACS Catal.* 9 (2019) 10649-10655.
- [35] H. Yu, Y. Xue, L. Hui, C. Zhang, Y. Fang, Y. Liu, X. Chen, D. Zhang, B. Huang, Y. Li, Graphdiyne based metal atomic catalysts for synthesizing ammonia. *Natl. Sci. Rev.* (2020) DOI: 10.1093/nsr/nwaa1213.

- [36] N. Wanninayake, Q. Ai, R. Zhou, M.A. Hoque, S. Herrell, M.I. Guzman, C. Risko, D.Y. Kim, Understanding the effect of host structure of nitrogen doped ultrananocrystalline diamond electrode on electrochemical carbon dioxide reduction. *Carbon* 157 (2020) 408-419.
- [37] M. Tomisaki, S. Kasahara, K. Natsui, N. Ikemiya, Y. Einaga, Switchable Product Selectivity in the Electrochemical Reduction of Carbon Dioxide Using Boron-Doped Diamond Electrodes. *J. Am. Chem. Soc.* 141 (2019) 7414-7420.
- [38] P.K. Jiwanti, K. Natsui, Y. Einaga, The Utilization of Boron-doped Diamond Electrodes for the Electrochemical Reduction of CO₂: Toward the Production of Compounds with a High Number of Carbon Atoms. *Electrochemistry* 87 (2019) 109-113.
- [39] K. Natsui, H. Iwakawa, N. Ikemiya, K. Nakata, Y. Einaga, Stable and Highly Efficient Electrochemical Production of Formic Acid from Carbon Dioxide Using Diamond Electrodes. *Angew. Chem. Int. Ed.* 57 (2018) 2639-2643.
- [40] C.J.H. Wort, R.S. Balmer, Diamond as an electronic material. *Mater. Today* 11 (2008) 22-28.
- [41] Y. Einaga, Diamond electrodes for electrochemical analysis. *J. Appl. Electrochem.* 40 (2010) 1807-1816.
- [42] B. Delley, From molecules to solids with the DMol3 approach. *J. Chem. Phys.* 113 (2000) 7756-7764.
- [43] B. Delley, An all-electron numerical method for solving the local density functional for polyatomic molecules. *J. Chem. Phys.* 92 (1990) 508-517.
- [44] B. Hammer, L.B. Hansen, J.K. Nørskov, Improved adsorption energetics within density-functional theory using revised Perdew-Burke-Ernzerhof functionals. *Phys. Rev. B* 59 (1999) 7413-7421.

- [45] M. Dolg, U. Wedig, H. Stoll, H. Preuss, Ab initio pseudopotential study of the first row transition metal monoxides and iron monohydride. *J. Chem. Phys.* 86 (1987) 2123-2131.
- [46] A. Bergner, M. Dolg, W. Küchle, H. Stoll, H. Preuß, Ab initio energy-adjusted pseudopotentials for elements of groups 13–17. *Mol. Phys.* 80 (2006) 1431-1441.
- [47] J. Rossmeisl, A. Logadottir, J.K. Nørskov, Electrolysis of water on (oxidized) metal surfaces. *Chem. Phys.* 319 (2005) 178-184.
- [48] A.A. Peterson, F. Abild-Pedersen, F. Studt, J. Rossmeisl, J.K. Nørskov, How copper catalyzes the electroreduction of carbon dioxide into hydrocarbon fuels. *Energy Environ. Sci.* 3 (2010) 1311-1315.
- [49] J.K. Nørskov, J. Rossmeisl, A. Logadottir, L. Lindqvist, J.R. Kitchin, T. Bligaard, H. Jónsson, Origin of the Overpotential for Oxygen Reduction at a Fuel-Cell Cathode. *J. Phys. Chem. B* 108 (2004) 17886-17892.
- [50] J.H. Montoya, C. Tsai, A. Vojvodic, J.K. Nørskov, The Challenge of Electrochemical Ammonia Synthesis: A New Perspective on the Role of Nitrogen Scaling Relations. *ChemSusChem* 8 (2015) 2180-2186.
- [51] F.L. Hirshfeld, Bonded-atom fragments for describing molecular charge densities. *Theor. Chim. Acta* 44 (1977) 129-138.
- [52] C. Lv, Y. Qian, C. Yan, Y. Ding, Y. Liu, G. Chen, G. Yu, Defect Engineering Metal-Free Polymeric Carbon Nitride Electrocatalyst for Effective Nitrogen Fixation under Ambient Conditions. *Angew. Chem. Int. Ed.* 57 (2018) 10246-10250.
- [53] H. Li, J. Shang, Z. Ai, L. Zhang, Efficient Visible Light Nitrogen Fixation with BiOBr Nanosheets of Oxygen Vacancies on the Exposed {001} Facets. *J. Am. Chem. Soc.* 137 (2015) 6393-6399.

- [54] X. Ren, J. Zhao, Q. Wei, Y. Ma, H. Guo, Q. Liu, Y. Wang, G. Cui, A.M. Asiri, B. Li, B. Tang, X. Sun, High-Performance N₂-to-NH₃ Conversion Electrocatalyzed by Mo₂C Nanorod. *ACS Cent. Sci.* 5 (2019) 116-121.
- [55] C. Chen, D. Yan, Y. Wang, Y. Zhou, Y. Zou, Y. Li, S. Wang, B-N Pairs Enriched Defective Carbon Nanosheets for Ammonia Synthesis with High Efficiency. *Small* 15 (2019) 1805029.
- [56] W. Guo, K. Zhang, Z. Liang, R. Zou, Q. Xu, Electrochemical nitrogen fixation and utilization: theories, advanced catalyst materials and system design. *Chem. Soc. Rev.* 48 (2019) 5658-5716.
- [57] S. Zhang, M. Jin, T. Shi, M. Han, Q. Sun, Y. Lin, Z. Ding, L.R. Zheng, G. Wang, Y. Zhang, H. Zhang, H. Zhao, Electrocatalytically Active Fe-(O-C₂)₄ Single-Atom Sites for Efficient Reduction of Nitrogen to Ammonia. *Angew. Chem. Int. Ed.* 59 (2020) 13423-13429.
- [58] E. Skúlason, T. Bligaard, S. Gudmundsdóttir, F. Studt, J. Rossmeisl, F. Abild-Pedersen, T. Vegge, H. Jónsson, J.K. Nørskov, A theoretical evaluation of possible transition metal electrocatalysts for N₂reduction. *Phys. Chem. Chem. Phys.* 14 (2012) 1235-1245.
- [59] C. Lv, Y. Qian, C. Yan, Y. Ding, Y. Liu, G. Chen, G. Yu, Defect Engineering Metal-Free Polymeric Carbon Nitride Electrocatalyst for Effective Nitrogen Fixation under Ambient Conditions. *Angew. Chem. Int. Ed.* 57 (2018) 10246-10250.
- [60] Á. Logadóttir, J.K. Nørskov, Ammonia synthesis over a Ru(0001) surface studied by density functional calculations. *J. Catal.* 220 (2003) 273-279.
- [61] C. Choi, S. Back, N.-Y. Kim, J. Lim, Y.-H. Kim, Y. Jung, Suppression of Hydrogen Evolution Reaction in Electrochemical N₂ Reduction Using Single-Atom Catalysts: A Computational Guideline. *ACS Catal.* 8 (2018) 7517-7525.

- [62] A.R. Singh, B.A. Rohr, J.A. Schwalbe, M. Cargnello, K. Chan, T.F. Jaramillo, I. Chorkendorff, J.K. Nørskov, Electrochemical Ammonia Synthesis—The Selectivity Challenge. *ACS Catal.* 7 (2016) 706-709.
- [63] D. Takeuchi, H. Kato, G.S. Ri, T. Yamada, P.R. Vinod, D. Hwang, C.E. Nebel, H. Okushi, S. Yamasaki, Direct observation of negative electron affinity in hydrogen-terminated diamond surfaces. *Appl. Phys. Lett.* 86 (2005) 152103.
- [64] J.R. Christianson, D. Zhu, R.J. Hamers, J.R. Schmidt, Mechanism of N₂ Reduction to NH₃ by Aqueous Solvated Electrons. *The Journal of Physical Chemistry B* 118 (2014) 195-203.
- [65] L. Zhang, D. Zhu, G.M. Nathanson, R.J. Hamers, Selective Photoelectrochemical Reduction of Aqueous CO₂ to CO by Solvated Electrons. *Angew. Chem. Int. Ed.* 53 (2014) 9746-9750.
- [66] T. Sun, F.A.M. Koeck, C. Zhu, R.J. Nemanich, Combined visible light photo-emission and low temperature thermionic emission from nitrogen doped diamond films. *Appl. Phys. Lett.* 99 (2011) 202101.

Author statement: Zhongyuan Guo, Siyao Qiu, Huan Li, Yongjun Xu, Steven J. Langford and Chenghua Sun conceived and designed the project and Zhongyuan Guo performed the DFT calculations. Zhongyuan Guo, Siyao Qiu, Huan Li, Yongjun Xu, Steven J. Langford and Chenghua Sun discussed the DFT results. Zhongyuan Guo wrote the original draft and Siyao Qiu, Huan Li, Yongjun Xu, Steven J. Langford and Chenghua Sun reviewed/edited it. Siyao Qiu, Steven J. Langford and Chenghua Sun supervised this project.

Journal Pre-proof

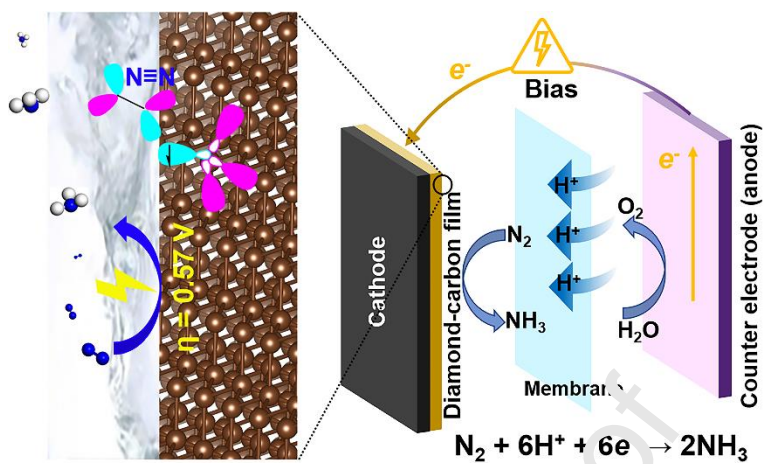
Declaration of interests

The authors declare that they have no known competing financial interests or personal relationships that could have appeared to influence the work reported in this paper.

The authors declare the following financial interests/personal relationships which may be considered as potential competing interests:

Journal Pre-proof

Graphical abstrac



Highlights:

- The effect of low-coordinated sp^3 -hybridized diamond-carbon showing activity towards eNRR is first investigated through DFT calculations.
- Two commonly exposed surface of diamond carbon, C(111) & C(110), are shown to be promising for dinitrogen reduction.
- C(111) exhibits the best activity towards eNRR with a low over-potential of just 0.57 V through the associative distal pathway.